Two-Dimensional (z-θ) Simulations of Hall Thruster Anomalous Transport

IEPC-2009-102

Presented at the 31st International Electric Propulsion Conference,
University of Michigan • Ann Arbor, Michigan • USA
September 20 – 24, 2009

Cheryl M. Lam[1], Aaron K. Knoll[2], and Mark A. Cappelli, [3]
High Temperature Gasdynamics Laboratory, Stanford University, Stanford, CA 94305-3032, USA

and

Eduardo Fernandez[4]
Department of Mathematics and Physics, Eckerd College, St. Petersburg, FL, 33711 94305

Abstract: This paper presents results on the development of both hybrid and multi-fluid simulations of Hall thrusters that resolve azimuthal electron flow dynamics. Simulations are carried out for a laboratory, nominally 90 mm channel diameter discharge with an extended acceleration region for which a modest collection of experimental data exists. The simulations are intended as a tool to better understand the mechanism behind azimuthal wave-driven electron transport. Both the hybrid and fluid simulations capture azimuthal fluctuations which appear to be consistent with quasi-neutral disturbances predicted by linear analysis. The impact of such disturbances on the cross-field transport is discussed.

Nomenclature

$\mu_\perp$	=	perpendicular electron mobility, based on classical scattering
ν_{en}, ν_{eN}	=	electron-neutral collision frequency
ω_{ce}	=	electron cyclotron frequency
θ	=	azimuthal coordinate direction
$\boldsymbol{B}$	=	magnetic field vector
B_r	=	radial component of magnetic field
$D_\perp$	=	perpendicular diffusion constant, based on classical scattering
dt	=	time step
e	=	magnitude of electron charge, 1.6×10^{-19} C
$\boldsymbol{E}$	=	electric field vector
E_θ	=	azimuthal component of electric field
E_z	=	axial component of electric field
k	=	Boltzmann constant, 1.38×10^{-23} m^2 kg s^{-2} K^{-1}
m_e	=	electron mass, 9.1×10^{-31} kg
n_e	=	electron number density
n_i	=	ion number density

[1] Graduate Research Assistant, Mechanical Engineering Department, cheryl16@stanford.edu.
[2] Graduate Research Assistant, Mechanical Engineering Department, aknoll@stanford.edu.
[3] Professor, Mechanical Engineering Department, cap@stanford.edu.
[4] Associate Professor, Department of Mathematics and Physics, fernane@eckerd.edu.

P_e = electron pressure, $n_e k T_e$
r = radial coordinate direction
t = time
T_e = electron temperature
$u_{e\theta}$ = azimuthal electron velocity
u_{ez} = axial electron velocity
$\dot{W}$ = production rate of electrons via ionization
z = axial coordinate direction

I. Introduction

THE possibility of anomalously high electron mobility across the magnetic field has been experimentally documented since the early years of Hall thruster development.[1,2] The mechanism leading to this anomalous mobility remains as one of the key challenges in Hall thruster research. A lack of understanding of what generates super-classical mobility in some regions of the flow, while being very near classical in other regions, has curtailed the usefulness of two-dimensional (2D) hybrid simulations in the radial-axial plane.[3-5] These simulations have provided qualitative insight into the operational behavior of thrusters of varying geometry, including wall erosion behavior.[6] However, in all existing simulations, transport must be adjusted in a rather ad-hoc fashion in order to obtain good agreement with even the simplest of performance parameters, such as the discharge current for a specified discharge voltage. Quite often, a "tuned" model for one operating condition is not transportable to another operating condition, or for that matter, another thruster geometry or thruster operating on an alternative propellant.

Some models attribute cross-field transport inside the thruster to electron scattering with the ceramic wall lining the discharge channel.[7] Others[4,8] use a Bohm type scaling for the mobility, which is motivated by the possible presence of high frequency quasi-coherent fluctuations resulting from instabilities within the plasma. The overarching goal of our research is to provide a sound basis for a transport description that can be imported into these potentially very useful 2D radial-axial (r-z) hybrid simulations. Without such a model, the performance, erosion, and ion trajectories (which are used in spacecraft integration) predicted by such simulations will always be in question. Recently[9], we proposed a transport description based on a polytropic model developed by assuming isentropic electron flow through the channel. This model has been tested in one-dimensional fluid simulations, and is still in the process of being imported into 2D r-z hybrid schemes. While this model shows some promise for future extension of these 2D simulations, the basis for this isentropic flow assumption is yet to be justified. In this paper, we focus on understanding the role played by fluctuations; particularly those that propagate with components perpendicular to both the applied electric ($\boldsymbol{E}$) and magnetic ($\boldsymbol{B}$) field, by means of numerical simulations that resolve the electron dynamics in the azimuthal direction, i.e., in the axial-azimuthal (z-θ) plane. Two independent z-θ simulations are under development in our group. One is a variant of the usual quasi-neutral hybrid simulations that treat the electrons as an inertialess fluid and the ions and neutrals as particles, but instead of resolving electron motion in the radial domain, it unfolds it azimuthally with periodic boundary conditions. The other is a fully three-fluid model of precisely the same geometry, but it retains the electron inertia terms. A brief description of the two models is provided below.

II. Simulation Description

As mentioned above, two independent z-θ simulations are under development, both of which can provide interesting and useful insight into the nature of the azimuthal electron dynamics in Hall thrusters. As far as we know, these are the first z-θ-resolved simulations of *entire thrusters*, starting with the anode region at the base to beyond the exit. A schematic illustration of the thruster, indicating the region of the flow that is simulated, is shown in Fig. 1.

The geometry simulated is that of a laboratory Hall discharge for which a considerable amount of experimental data has been gathered.[2,10] The discharge has an annular channel 8 cm in length and 1.2 cm in width, and

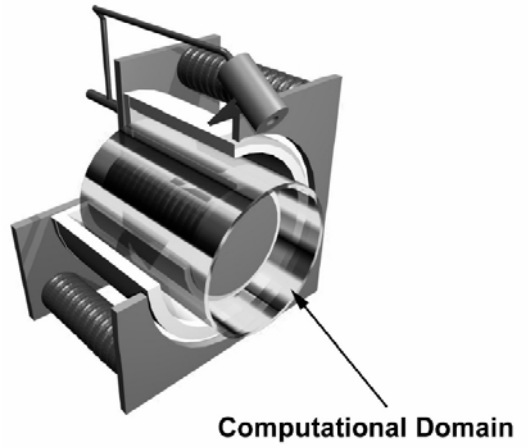

Figure 1. Schematic of the thruster modeled and the computational domain.

an outer diameter of approximately 9 cm. The predominantly radial magnetic field peaks at a value of about B_r=.01 T just upstream of the channel exit.

The axial electric field is imposed by a positive voltage (relative to 0 V) applied at the anode. If we treat the magnetic field as purely radial, this gives an $\boldsymbol{E} \times \boldsymbol{B}$ drift velocity in the purely azimuthal direction. In both simulations, the 2D z-θ coordinate system is oriented such that the $\boldsymbol{E} \times \boldsymbol{B}$ drift velocity is in the positive θ-direction

A. Hybrid Simulation

As in the several versions of hybrid simulations employed to study the structure of Hall thruster plasmas in the r-z plane, the z-θ simulation tracks ions and neutrals as particles, and the electrons as a fluid. The magnetic field is assumed to be in the radial direction, and uses the magnetic field measured in the SHT along the z axis at a midway radial location. The electron fluid is governed by continuity, momentum, and energy equations. These equations are essentially those used in the r-z description, except that they now incorporate the azimuthal terms. The electron momentum is described by drift-diffusion as before; however, the model now has two cross field electron velocity components, one in the axial direction, and the other in the azimuthal direction:

$$u_{e_z} = -\mu_\perp E_z - \frac{D_\perp}{n_e}\frac{\partial n_e}{\partial z} - \frac{D_\perp}{T_e}\frac{\partial T_e}{\partial z} - \frac{1}{1+\left(\frac{\nu_{en}}{\omega_{ce}}\right)^2}\frac{E_\theta}{B_r} - \frac{1}{1+\left(\frac{\nu_{en}}{\omega_{ce}}\right)^2}\frac{kT_e}{en_eB_r r}\frac{\partial n_e}{\partial \theta} \tag{1.1}$$

$$u_{e_\theta} = -\mu_\perp E_\theta - \frac{D_\perp}{n_e r}\frac{\partial n_e}{\partial \theta} + \frac{1}{1+\left(\frac{\nu_{en}}{\omega_{ce}}\right)^2}\frac{E_z}{B_r} + \frac{1}{1+\left(\frac{\nu_{en}}{\omega_{ce}}\right)^2}\frac{kT_e}{en_eB_r}\frac{\partial n_e}{\partial z} + \frac{1}{1+\left(\frac{\nu_{en}}{\omega_{ce}}\right)^2}\frac{k}{eB_r}\frac{\partial T_e}{\partial z} \tag{1.2}$$

To see how fluctuation-induced transport can occur, we note that the axial velocity has a fluctuating $\boldsymbol{E} \times \boldsymbol{B}$ term arising from azimuthal electric field perturbations. If the fluctuating plasma density is properly correlated with this fluctuating velocity, transport will result. We note that in the present version of the model, electron inertia terms are neglected.

Electron energy is described by a time-dependent equation with the same physics as the r-z model: it has convective and diffusive fluxes, joule heating, ionization losses and an effective wall loss term. The electron energy equation is one-dimensional in z; the electron temperature is, thus, taken to be axisymmetric.

Neutral xenon atoms are treated as particles and are ionized according to the local ionization rate. The ionization rate depends nonlinearly on electron temperature, and it is determined from fits using experimental cross sections and assuming a Maxwellian distribution for the electrons. Neutral atoms are injected in the domain according to the mass flow rate. The ions, also treated as particles, are assumed to be non-magnetized and only respond to the electrostatic electric field. Since the simulation has no radial physics (for example, there is no radial velocity for electrons, ions or neutrals) effects like wall collisions have to be modeled. For the results presented below, ion and neutral collisions with the wall are not included. The neutral injection velocity is sampled from a half-Maxwellian distribution, centered at a mean speed chosen to best match conditions seen along the channel centerline in similar r-z simulations which do include wall collision effects.

The computational grid is non-uniform in the axial direction, with adjustable grid clustering around the peak of the magnetic field, where gradients are expected to be large. The grid is uniform in the periodic azimuthal direction. In an effort to balance resolution and computational cost, an initial grid of 40 (axial) by 50 (azimuthal) points is used. The axial domain extends from the anode to four centimeters past the channel exit.

The time-dependent electron temperature equation is solved via a fourth-order Runge-Kutta scheme. The electric field is not solved from Poisson's equation (since quasineutrality is assumed) and, instead, is obtained from combining the continuity and momentum equations and setting $n_e = n_i$. The heavy particles are advanced using a leap frog method and interpolated electric field; they are advanced with the same time step as the electrons. At each step, some neutrals are injected at the anode based on the mass flow rate. Neutrals are also ionized at each step according to the local ionization rate. This sequence of steps is repeated after a steady-state for the mean quantities is obtained. The steady-state is non-stationary; sustained electric current discharge oscillations are a distinctive feature of the simulation.

In the z-θ model, the electric potential is obtained by solving a convection-diffusion equation that results from combining the current continuity and momentum equations. The difficulty with this equation is the strong convection imposed by the electron $\boldsymbol{E} \times \boldsymbol{B}$ flow. We use a high-order upwind discretization method[11] in order to circumvent numerical instability. Such discretization results in a block-tridiagonal matrix for the electric potential

that is solved via a direct-solve method. The boundary conditions are periodic in the azimuthal direction and Dirichlet in the axial direction. While the Dirichlet boundary condition at the anode is reasonable (the anode is at a fixed voltage), the downstream boundary condition is less clear. Presently, the electric potential is set equal to that measured experimentally at the downstream boundary (four centimeters past the channel exit).

B. Fluid Simulation

In addition to the hybrid simulation described above, a fully fluid simulation has been developed in the z-θ coordinates of the Hall thruster. This simulation models the electrons, ions, and neutral particles as three independent fluid continuums. This simulation tracks ten unknowns in two-dimensional space: the velocity components of each fluid, the number density of the electrons and ions (which are explicitly set equal to each other), the neutral number density, the plasma potential, and the plasma temperature. These unknowns are advanced in time by a system of ten equations: conservation and momentum equations for the electrons, ions, and neutral particles, as well as an energy equation which, like the hybrid model, has convective and diffusive fluxes, joule heating, ionization losses and an effective wall loss term. The electron momentum equations are somewhat different than those used in the hybrid simulation. These equations include transient and non-linear electron inertia contributions that are neglected in the hybrid model. These equations are given by

$$\frac{\partial u_{ez}}{\partial t} + u_{ez}\frac{\partial u_{ez}}{\partial z} + \frac{u_{e\theta}}{r}\frac{\partial u_{ez}}{\partial \theta} = -\frac{1}{n_e m_e}\frac{\partial P_e}{\partial z} - \frac{e}{m_e}(E_z + u_{e\theta}B_r) - \nu_{eN}u_{ez} - \frac{u_{ez}\dot{W}}{n_e}, \text{ and} \tag{1.3}$$

$$\frac{\partial u_{e\theta}}{\partial t} + u_{ez}\frac{\partial u_{e\theta}}{\partial z} + \frac{u_{e\theta}}{r}\frac{\partial u_{e\theta}}{\partial \theta} = -\frac{1}{n_e m_e r}\frac{\partial P_e}{\partial \theta} - \frac{e}{m_e}(E_\theta - u_{ez}B_r) - \nu_{eN}u_{e\theta} - \frac{u_{e\theta}\dot{W}}{n_e}. \tag{1.4}$$

The addition of the non-linear electron inertia and transient terms to the electron momentum equations allow high frequency instabilities on the order of 100MHz and higher to be captured. The impact that these very high frequency instabilities may have on the electron transport process are a matter of interest, as discussed above.[12,13] Also, these terms provide a direct means of coupling energy from one wave mode to another. For example, energy from axial instabilities can feed azimuthally propagating waves through non-linear three-wave coupling. Although the relative magnitude of the electron inertia terms are small compared to other terms in the equation, their contribution may prove to be vital in transferring energy between different instabilities.

The governing equations for the fluid simulation are discretized on a grid of 25 axial by 70 azimuthal computational points. This grid is uniform in both the axial and azimuthal directions. The physical region of the simulation extends from the anode to 2 cm downstream of the thruster exit, and includes the full azimuth of the channel. Spatial discretization and time advancement follow a predictor-corrector iteration technique similar to the MacCormack method.[14] However, this technique differs from the MacCormack method in the choice of the time advancement function. This simulation uses an implicit 2nd-order backward difference technique as opposed to the explicit 1st-order forward difference technique used by the traditional MacCormack approach. The implicit formulation allows a greater range of stability conditions compared to the traditional MacCormack method, while still using the predictor-corrector strategy to allow the simulation to handle mixed systems of hyperbolic and elliptic equations. Stability analysis indicates that this method is, in fact, unconditionally stable for linear problems. However, it should be noted that non-linearity in the system of equations can, in principle, make the time advancement unstable. So far this method has proved stable and successful for the plasma dynamic equations described above, using a time step size of 1 ns.

In comparison to the hybrid simulation, the fully fluid model offers certain advantages as well as some disadvantages. One main advantage, as has been discussed previously, is that the full fluid model described here retains terms in the electron momentum equation related to the electron inertia. This allows the simulation to capture non-linear wave coupling and instabilities at linear frequencies of 100 MHz and above, that are not captured in the hybrid simulation. Another advantage is that the fluid simulation provides a one-to-one correspondence to equations often used to develop linear wave dispersion relations, such as in the work of Thomas.[15] The fluid model also allows terms in the equations to be turned on and off; the effect of these changes can be observed directly from the simulation results for possible comparison to the hybrid model. This also allows the simulation to be used as a tool to easily identify the mechanisms leading to instability and to provide a direct means of calculating the contribution of these instabilities to the electron transport.

The fluid simulation also has certain disadvantages compared to the hybrid model. The fluid model has a higher computational complexity and takes longer to run than the hybrid code, roughly by a factor of 10. Also, certain physical phenomena are better modeled by the hybrid code, such as capturing non-Maxwellian velocity distributions for both the neutral particles and ions. In short, the hybrid code is faster and more representative of Hall thruster experiments, whereas the fluid model is slower but may be more useful at studying instabilities and associated transport. The results of each simulation are compared below.

III. Results

A. General Results

Hybrid and fluid simulations were performed for the described geometry; here, the simulation results are examined and compared to experimental measurements of plasma properties at the given operating conditions.

The hybrid simulation was initialized by assigning a uniform number of particles to each cell, with the particles randomly distributed in position within each cell; the particle velocities were initialized by inverting a Maxwellian velocity distribution. A 200 μs simulation was performed, using a timestep of 1 ns; the simulation took approximately 6 days to complete on a single Intel Xeon x5355 2.66GHz processor core.

Initial conditions for the 2D fluid simulation were established by running an axisymmetric simulation to steady-state, by setting all the time-derivatives to zero. The results of this axisymmetric, steady-state simulation were then used as the initial conditions for the 2D fluid simulation. A 1 μs run was performed, using a timestep of 1 ns; the simulation took approximately 8 hours to complete on a single Intel 5454 Xeon x64 3.0GHz processor core (not including the initial simulation time to establish initial conditions).

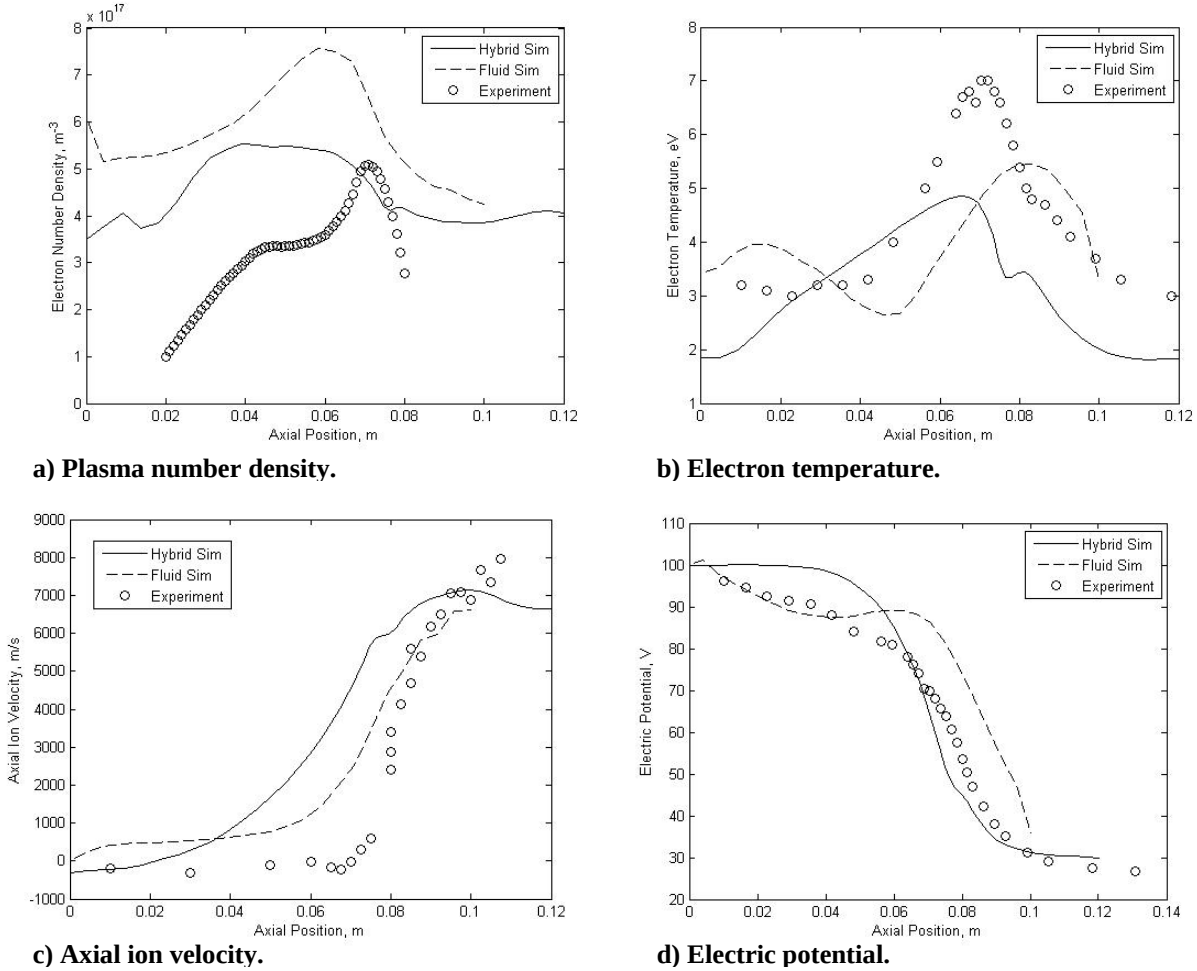

a) Plasma number density. **b) Electron temperature.**

c) Axial ion velocity. **d) Electric potential.**

Figure 2. Comparison of time-averaged axial profiles for various plasma properties.

In both simulations, the operating voltage is imposed through axisymmetric Dirichlet boundary conditions at the anode (z = 0 m) and at the end of the domain (z = 0.12 m and z = 0.1 m, respectively, for the hybrid and the fluid). Both simulations were performed for an operating voltage of 100V. In both simulations, the discharge current varies slightly with axial location and time. The hybrid simulation predicts a discharge current of 1-2 A. The fluid simulation predicts a discharge current of 2.5-4 A. In experiments at this operating voltage, the measured discharge current was approximately 2 A. For both simulations, a mass flow rate of 2 mg/s was imposed, to approximately match experimental operating conditions.

Fig. 2 shows the time-averaged axial profiles of various plasma properties: electron number density (or plasma density), electric potential, electron temperature, and axial ion velocity. For the hybrid simulation, the time average was taken over the time duration 50 μs to 100 μs; for the fluid simulation, the entire 1 μs time duration was used. In general, the simulated axial profiles show good qualitative and order of magnitude agreement with experimental measurements.

Closer analysis of the simulation results reveals dispersive wave propagation; the wave properties (wavenumber, frequency, phase velocity, and propagation direction) appear to vary with axial position. As expected, the hybrid simulation predicts slower, lower frequency waves, while the fluid simulation indicates faster, high frequency wave behavior.

B. Wave Propagation in Hybrid Simulation

The extended time duration of the hybrid simulation allows for investigation of low frequency fluctuations. In the plasma number density, we observe a very low frequency axially-propagating disturbance across all azimuthal positions for all axial positions inside the thruster channel (0 m < z ≤ 0.08 m). Over the 200 μs simulation, this disturbance appears as a distinct increase, then decrease, in plasma density magnitude across all azimuthal positions; longer simulations would be needed to confirm the time periodicity of this disturbance. Fig. 3 is typical of the behavior observed throughout the thruster channel; from these so-called streak plots, we infer a linear frequency on the order of 10 KHz. This low frequency plasma density wave is highly reminiscent of the experimentally observed 20 KHz breathing mode.

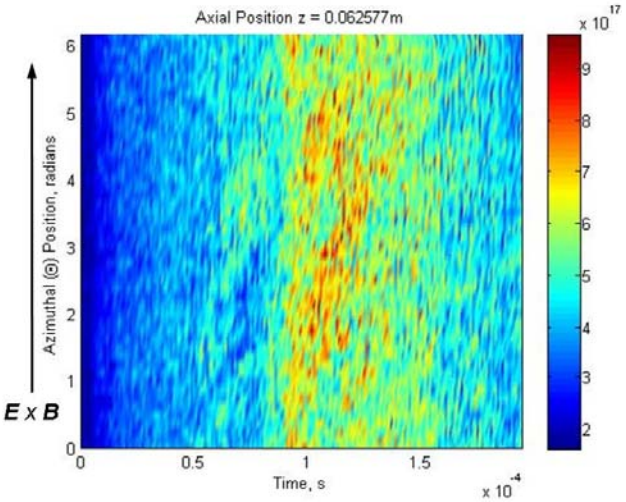

Figure 3. Plasma number density streak plot at axial location z = 0.06257 m.

In addition to this axially-pervasive, low frequency, breathing mode-like behavior, we observe tilted waves which propagate simultaneously in the axial and azimuthal directions. The structure, speed and direction of these tilted waves appear to vary with axial position. Fig. 5b is representative of the spatial variation in wave structure. In Figs. 4-7, we present a time snapshot and streak plots of the axial electron velocity to illustrate the spatial wave structure and variation of wave properties with axial position. Although not shown here, we observe similar wave structure, with axial position, in the plasma density and electric potential.

As illustrated in Fig. 5b, we observe distinct wave behavior in three distinct axial regions. For most of the thruster channel, starting just downstream of the anode to just upstream of the channel exit plane (approximately, 0.01 m ≤ z ≤ 0.07m), we observe tilted waves, propagating in the negative z- and positive θ-directions. Streak plots, such as Fig. 4, in this axial region reveal the time variation of the wave structure. These waves have an azimuthal wavelength on the order of 5 cm and a linear frequency of approximately 40 KHz; the phase velocity is approximately 4000 m/s. These waves are low frequency and slow moving, and travel in the **+** ***E*** x ***B*** direction.

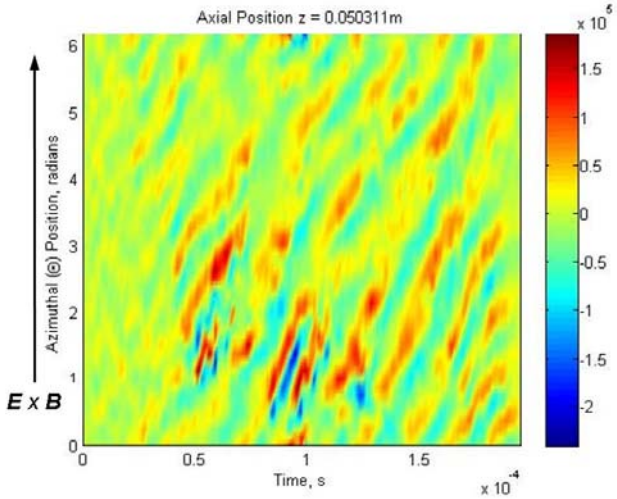

Figure 4. Axial electron velocity streak plot at axial location z = 0.05031 m.

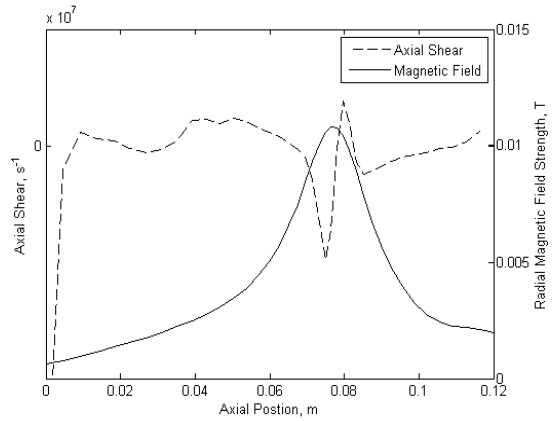

a) Variation of radial magnetic field strength B_r and axial shear $\partial u_{e\theta}/\partial z$ with axial position.

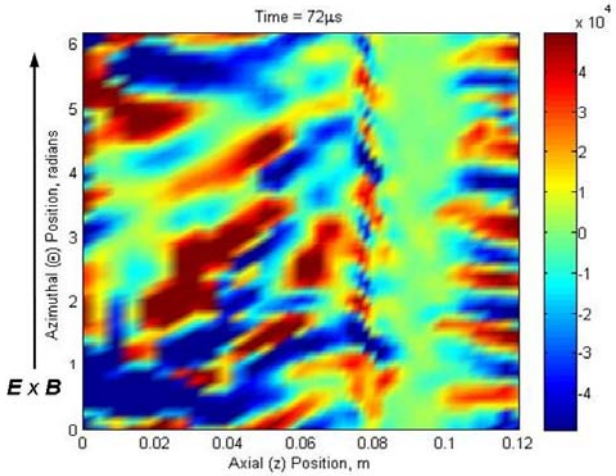

b) Representative time snapshot of axial electron velocity v_{ez}, taken 72 μs into the hybrid simulation.

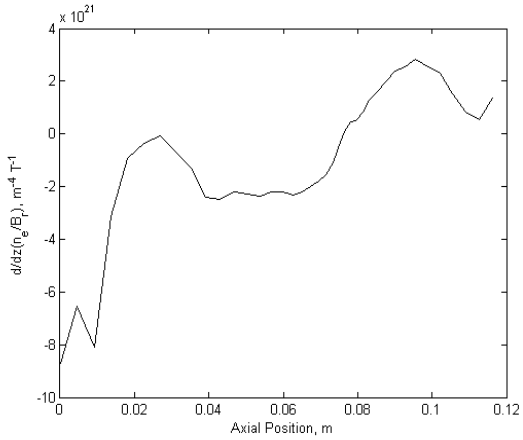

c) Axial gradient of n_e/B_r.

Figure 5. A typical time snapshot of the axial electron velocity illustrates the spatial structure of wave propagation, as related to axial variation of the magnetic field strength, shear and n_e/B_r gradient.

In a narrow axial region (approximately, 0.07 m ≤ z ≤ 0.08 m), starting just upstream of the thruster channel exit plane through the exit plane itself, we observe higher frequency, tilted waves traveling in the positive z- and negative θ-directions. Over long time scales, as shown in Fig. 6a, the coherent wave structure cannot be discerned; instead, the behavior appears turbulent with indiscernible high frequency structure. Examination at shorter time scales, as in Fig. 6b, however, reveals fast-moving waves. These waves have an azimuthal wavelength on the order of 4 cm and a linear frequency on the order of 600-700 KHz; the phase velocity is approximately 40,000 m/s. These waves are shorter wavelength, higher frequency and faster moving (than the waves in the upstream region 0.01 m ≤ z ≤ 0.07 m); they travel in the **- *E* x *B*** direction. We note

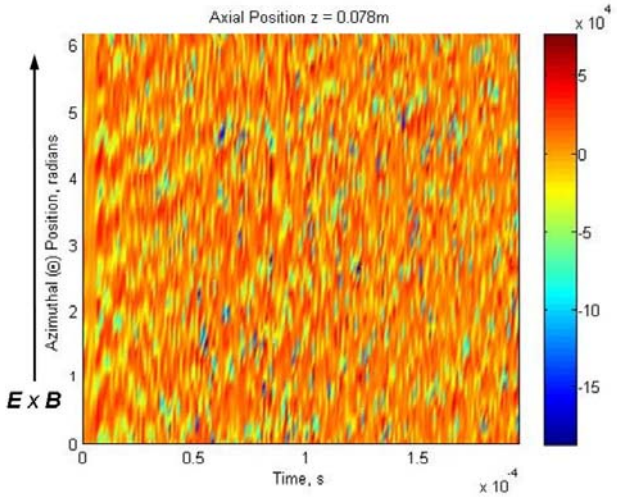

a) Low time-resolution streak plot, shown over the full 200 μs simulation time duration.

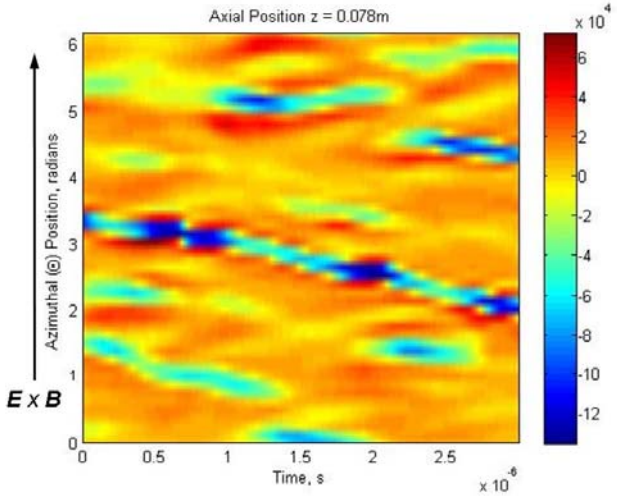

b) High time-resolution (ns sampling rate) streak plot, shown over a time duration of 3 μs.

Figure 6. Axial electron velocity streak plot at axial location *z* = 0.078 m, shown at different time scales.

that this axial region corresponds to the region of peak magnetic field strength; as shown in Fig. 5a there is also a strong fluctuation and two opposite extremums (local maximum and local minimum) in the axial shear (of the azimuthal electron velocity) in this region. As shown in Fig. 5c, this is also the region in which the gradient of n_e/B_r becomes positive; i.e, the quantity n_e/B_r starts to increase near z = .075 m.

Just outside the exit plane, the wave structure is unclear. From approximately 10 cm past the exit plane through the end of the computational domain (z > 0.01 m), however, we observe waves propagating in the purely axial direction. These waves appear to have the same spatial structure and azimuthal wavelength as the waves just inside (and leaving) the thruster exit plane; they propagate in the positive z direction. A representative streak plot, as in Fig. 7, confirms the time persistence and purely axial nature of these waves.

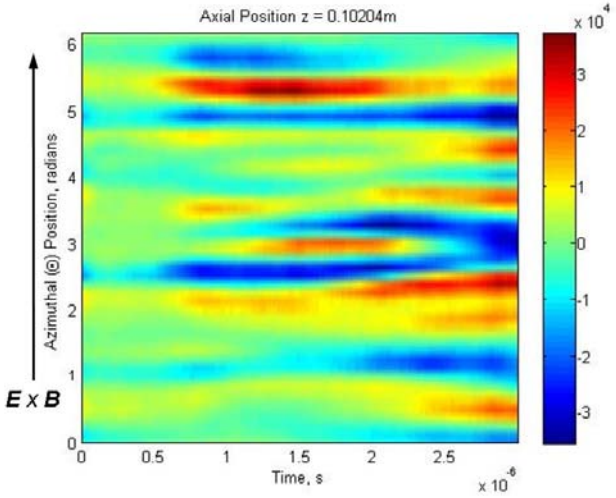

Figure 7. Axial electron velocity streak plot at axial location z = 0.102 m, shown at high time-resolution (ns sampling rate) over a time duration of 3 μs.

As detailed here, the wave structure varies distinctly with axial location; these changes in wave structure appear to be coincident with the axial variation of the magnetic field strength, axial shear, and gradient of n_e/B_r. The longer wavelength, lower frequency tilted waves, propagating in the negative z and **+** $\boldsymbol{E}$ x $\boldsymbol{B}$ direction, in the upstream axial region (0.01 m ≤ z ≤ 0.07 m), coincide with increasing magnetic field strength and low axial variation in the shear. We also note that in the region 0.4 m ≤ z ≤ 0.6 m, where these waves are most clear and coherent, the gradient of is n_e/B_r is nearly constant (and negative). At approximately z = 0.07 m, the waves reverse both axial and azimuthal propagation direction; the wavelength decreases, as the frequency and phase velocity increase by approximately one order of magnitude. As previously noted, these waves are coincident with peak magnetic field strength, strong axial variation in the axial shear, and a change in sign of the n_e/B_r gradient. The azimuthal spatial wave structure is then preserved as the waves are advected out of the thruster channel. Purely axial waves, propagating in the positive axial direction, can be observed downstream of the exit plane (for $z \geq$ 0.1 m); these waves appear to have the same azimuthal wavelength as those leaving the channel exit plane.

C. Wave Propagation in Fluid Simulation

From the fluid simulation results, we observe fast moving, high frequency tilted waves. The waves are axially-pervasive throughout the thruster channel, and are easily observed in the region 0.02 m ≤ z ≤ 0.08 m. Fig. 8 shows the spatial structure of these disturbances, while Fig. 9 illustrates the rapid temporal nature of these waves. These waves appear to propagate in the positive z- and negative θ-directions. They have an azimuthal wavelength on the order of 6 cm and a linear frequency on the order of 5 MHz; the phase velocity is approximately 300,000 m/s. While the azimuthal wavelength of these waves is of the same order as those observed in the hybrid simulation, the frequency and phase velocity are significantly higher. These waves travel in the **-** $\boldsymbol{E}$ x $\boldsymbol{B}$ direction.

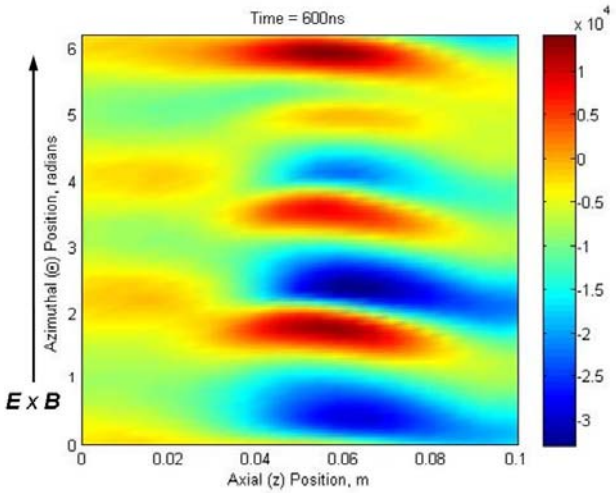

Figure 8. Representative time snapshot of axial electron velocity v_{ez}, taken 0.6 μs into the fluid simulation.

Compared to the hybrid, the fluid simulation predicts much higher frequency, faster-moving waves. In theory, the simulation timestep determines the time resolution of the predicted behavior; since the hybrid and fluid simulations are advanced using the same timestep (dt = 1 ns), they should be able to resolve the same temporal behavior and wave structure. We attribute this difference in predicted wave behavior, then, to the

difference in model formulations. As previously discussed, the fluid model retains the inertial terms in the electron momentum equations; we believe these terms may be significant in the prediction and study of high frequency instabilities.

D. Electron Transport

We are interested in the impact of azimuthal fluctuations on axial electron transport. Experimental measurements indicate an axial electron mobility significantly higher than that predicted by classical theory. It has been proposed that correlated fluctuations in the plasma density and electron velocity can enhance the axial electron mobility. In Fig. 10, we compare the axial electron mobility, predicted by the hybrid and fluid simulations; in each case, the classical mobility (based on predicted neutral number density and electron temperature) is shown for reference. In the hybrid simulation, the observed fluctuations in plasma density and electron velocity appear to have significant impact on the overall electron mobility. The electron mobility is significantly enhanced, compared to classical, at all axial locations; overall, the predicted mobility is of the same order of magnitude and shows good qualitative agreement with the experimentally-observed values. The fluid simulation also predicts an electron mobility on the same order as the experimentally-observed values; this predicted mobility is significantly higher than the predicted classical mobility for most axial locations. In the fluid simulation, we calculate the predicted mobility by time averaging over the entire 1 μs simulation time duration; we attribute the unusual structure in the electron mobility's axial variation to numerical error and instability, manifested as extreme fluctuations in the axial electric field E_z over time and axial location.

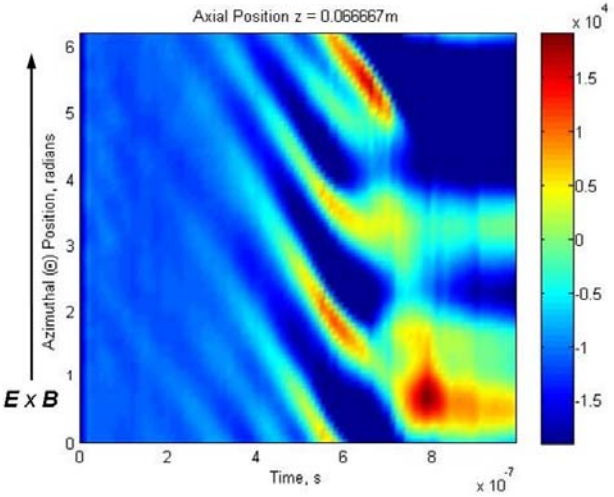

Figure 9. Axial electron velocity streak plot at axial location z = 0.067 m, shown over the full fluid simulation time duration of 1 μs.

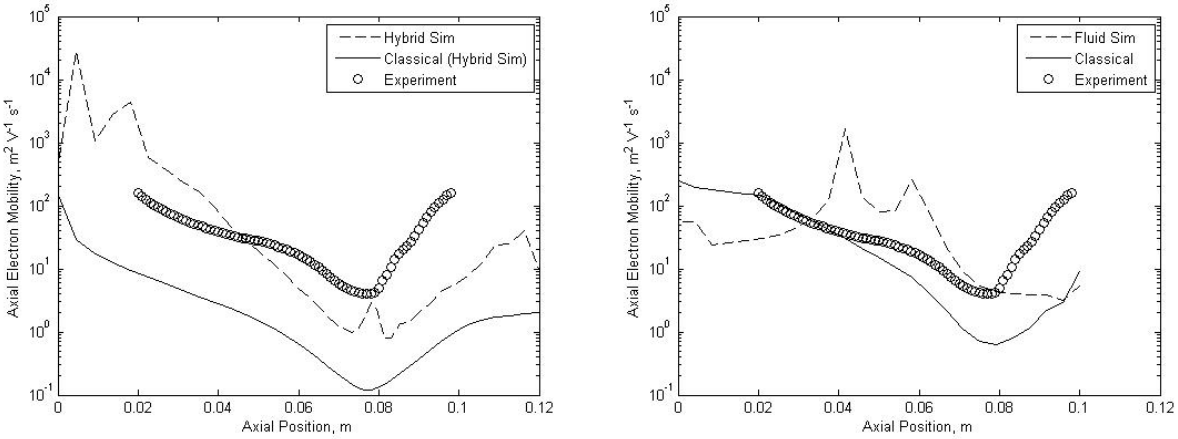

a) Hybrid simulation. **b) Fluid simulation.**

Figure 10. Comparison of predicted electron axial mobility, as compared to experimentally-measured and classically-predicted values.

IV. Conclusion

The approach taken here, i.e., the parallel development of both hybrid and multi-fluid simulations of Hall thrusters that resolve azimuthal electron flow dynamics is intended as an exercise in the development of fundamental understandings of how such azimuthal fluctuations may impact transport. We believe that we have developed the first simulations on full-scale (90 mm diameter) thrusters, with the azimuthal scale resolved in its entirety. However, simulations have been generally difficult to evolve beyond a few microseconds, in the case of the

fluid simulations, and a few hundred microseconds, in the case of the hybrid simulations. Both simulations predict the presence of strong azimuthal disturbances, that are generally complex; in some cases, such as in the hybrid simulations, these disturbances degrade spatially along the thruster axis, depending on the nature of the time-average properties, such as plasma density, magnetic field, and axial electron shear. The azimuthal waves predicted by both simulations have vastly different propagation characteristics, with the fluid model capturing waves of much higher frequency and phase velocity. We attribute these differences to differences in the modeling of the electron flow. The fluid simulation includes terms associated with the electron inertia, which are expected to be small in magnitude, but can provide a non-linear mechanism for energy coupling amongst dynamical modes of the system. The result is that both simulations, despite their differences in predicted wave propagation, predict an axial electron mobility that is significantly higher than that based on classical scattering; in both cases, the predicted mobility is qualitatively comparable to that seen in experiments.

Acknowledgments

This research was supported by the Air Force Office of Scientific Research, with Dr. Mitat Birkan as Program Manager. Tuition and stipend support for C. M. Lam was provided by Sandia National Laboratories.

References

[1]Janes, G. S. and Lowder, R. S., "Anomalous Electron Diffusion and Ion Acceleration in a Low-Density Plasma," *Phys. Fluids* ***9***, 1115, 1966.

[2]Meezan, N. B., Hargus, W.A., Jr., and Cappelli, M. A., "Anomalous electron mobility in a coaxial Hall discharge plasma," *Physical Review*, Vol. 63, No. 2, 026410, 2001.

[3]Fernandez, E., Cappelli, M. A., and Mahesh, K., "2D simulations of Hall thrusters," *Center for Turbulence Research Annual Research Briefs*, Stanford Univ., Stanford, CA. 1998, pp.81-90.

[4]Fife, J. M., "Hybrid-PIC modeling and electrostatic probe survey of Hall thrusters," Ph.D. Dissertation, Dept. of Aeronautics and Astronautics, Massachusetts Inst. of Technology, Cambridge, MA, 1999.

[5]Hagelaar, G. J. M, Bareilles, J., Garrigues, L., and Boeuf, J. -P., "Two-dimensional model of a stationary plasma thruster," *J. Appl. Phys.*, Vol. 91, No. 9, 5592, 2002.

[6]Sommier, E., Allis, M. K., and Cappelli, M.A., "Wall Erosion in 2D Hall Thruster Simulations," *29th International Electric Propulsion Conference*, Princeton Univ., Princeton, NJ, Oct. 31-Nov.4, 2005.

[7]Barral, S., Makowski, K., Peradzynski, Z., Gascon, N., and Dudeck, M., "Wall Material Effects in Stationary Plasma Thrusters. II Near-Wall and In-Wall Conductivity," *J. Physics of Plasmas.*, Vol. 10, No. 10, 4137, 2003.

[8]Scharfe, M. K., Gascon, N., and Cappelli, M. A., "Comparison of hybrid hall thruster model to experimental measurements," *Phys. Plasmas*, Vol. 13, No. 8, 083505, 2006.

[9]Knoll, A. K. and Cappelli, M. A., "A simple isentropic model of electron transport in Hall thrusters," *J. Phys.D: Appl. Phys.* ***41***, 162003, 2008.

[10]Hargus, W. A., "Investigation of the plasma acceleration mechanism within a coaxial Hall thruster," Ph.D. Disseration, Mechanical Engineering Dept., Stanford Univ., Stanford, CA, 2001.

[11]Fletcher, C. A. J., *Computational Techniques for Fluid Dynamics 1*, 2nd ed., Springer-Verlag, New York, 1991.

[12]Adam, J. C., Héron, A. and Laval, G., "Study of stationary plasma thrusters using two-dimensional fully kinetic simulations," *Phys. Plasmas*, Vol. 11, No. 1, 295, 2004.

[13]Ducrocq, A., Adam, J. C., Héron, A. and Laval, G., "High-frequency electron drift instability in the cross-field configuration of Hall thrusters," *Phys. Plasmas*, Vol. 13, No. 10, 10211, 2006.

[14]MacCormack, R. W., "The Effect of viscosity in hypervelocity impact cratering," *AIAA Paper*, 69-354, 1969.

[15]Thomas, C. A., "Anomalous electron transport in the Hall-effect thruster," Ph.D. Dissertation, Mechanical Engineering Dept., Stanford Univ., Stanford, CA, 2006.